Editors' Suggestion

Tubular-body theory for viscous flows

Lyndon Koens*
Department of Mathematics and Statistics, Macquarie University, Sydney, New South Wales 2113, Australia and Department of Physics and Mathematics, University of Hull, Hull HU6 7RX, United Kingdom

(Received 31 October 2021; accepted 7 February 2022; published 10 March 2022)

Cablelike bodies play a key role in many interdisciplinary systems but are hard to simulate. Asymptotic theories, called slender-body theories, are effective but apply in specific regimes and can be hard to extend beyond leading order. In this paper we develop an exact slender-body-like theory for the surface traction of cablelike bodies in viscous flow. This theory expresses the traction as a series of solutions to a well-behaved one-dimensional Fredholm integral equation of the second kind. This process can be simply generalized to other systems.

DOI: 10.1103/PhysRevFluids.7.034101

I. INTRODUCTION

Wiry objects are important to many systems: Spermatozoa and bacteria actuate slender appendages called flagella to swim [1,2]; eukaryotic cells change and maintain their shape with microtubules and actin filaments [3]; clays are colloids of electrically charged ribbons [4]; and fiber-reinforced plastics are light weight metamaterials that can be used for machine parts [5]. Systems with cablelike bodies often display complex and emergent behaviors but have internal structures that are hard to probe experimentally [6]. As a result theoretical and numerical models are needed to complement the experiments and improve understanding.

Unfortunately, the direct numerical simulation of tubelike bodies is often computationally heavy [7]. This is because the thickness of each body may be much smaller than its length and so a high resolution is required. Asymptotic theories, called slender-body theories (SBTs), have been developed to overcome this. These models exploit the separation in length scales to create an approximation for the behavior [8]. This process often reduces the model to a system of one-dimensional equations, thereby also increasing the computational efficiency.

Slender-body theory has been used in many fields with one of the most successful examples coming from slow-viscous flows. SBT for viscous flows has accurately modeled microscopic swimmers [1,2], flexible filaments [9], and settling rods [10]. In its most popular form, it expresses the force per unit length on an isolated filament through a one-dimensional integral equation [11–14]. Although the kernel of this operator is singular, this singularity asymptotically cancels with a "local" term. Even so, this model can be difficult to implement numerically and is known to suffer from high eigenvalue instabilities [10,14,15].

The approximate nature of SBTs typically restricts their use to specific regimes. Most assume that the thickness of the body is much less than all other length scales in the problem [10,16–18], although some restrict certain lengths to be similar to or smaller than the thickness [16,19,20]. Only one example exists without such a condition to our knowledge [7]. However, it restricts the geometry to that of a rod perpendicular to a wall. Furthermore, most SBTs are hard to extend beyond leading order [12,21]. Yet effective models without such limitations are needed.

*lyndon.koens@mq.edu.au; L. M.Koens@hull.ac.uk

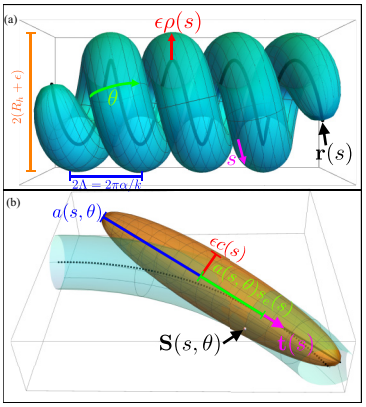

FIG. 1. (a) A tightly wound helix has a locally tubular structure. $\mathbf{r}(s)$ (black) is the centerline; $\epsilon\rho(s)$ (red) is the thickness; Λ (blue) is the helix pitch; R_h (orange) is the helix radius. The plot uses $\epsilon = 0.05$, $\Lambda = 1.1\epsilon$, and $R_h = 1.5\epsilon$. (b) The effective spheroid used to replicate the surface around $\mathbf{S}(s,\theta)$. $a(s,\theta)$ (blue) is the distance from the center to the pole along the symmetry axis, $\epsilon c(s)$ (red) is the equatorial radius, and $a(s,\theta)s_\epsilon(s)$ (green) is the distance from the center to $\mathbf{r}(s)$ along the tangent (magenta). These parameters are chosen such that the surface point and tangent plane match at $\mathbf{S}(s,\theta)$.

Realistic systems are dynamic and complex with wiry bodies changing shape, interacting with walls, and each other. This has been identified as a key issue in interdisciplinary research within reviews [9,20,22] and a Nat. Phys. Comment [23].

In this paper we develop tubular-body theory (TBT) for viscous flow. TBT is a SBT-like theory which exactly determines the traction on the surface of cablelike bodies. The theory is found by adding and subtracting the solution to an effective sphereoid to the singular-layer boundary integral representation and then expanding the system using a binomial series. Rearranging these equations, the traction is expressed as a series of solutions to a one-dimensional Fredholm integral equation of the second kind with a compact and self-adjoint kernel. This enables TBT to retain many of the computational advantages of SBT without the limitations. These equations are found to capture the behavior of spheroids and tori well outside classical SBT limits and simulate the motion of a tightly wound helix.

II. TUBULAR-BODY THEORY

Consider the behavior of tubular bodies in incompressible viscous flow [Fig. 1(a)]. The surface of these bodies can be written as

$$\mathbf{S}(s,\theta) = \mathbf{r}(s) + \epsilon\rho(s)\hat{\mathbf{e}}_\rho(s,\theta), \tag{1}$$

where $\mathbf{r}(s)$ is the centerline of the body parametrized by the arclength $s \in [-1, 1]$, $\epsilon\rho(s) \in [0, 1]$ is the thickness of the body at s, and $\hat{\mathbf{e}}_\rho(s,\theta)$ is the local radial vector perpendicular to the centerline tangent $\partial_s\mathbf{r}(s) = \hat{\mathbf{t}}(s)$. Without any loss of generality we choose $\hat{\mathbf{e}}_\rho(s,\theta)$ to be parametrized such that $\partial_s\hat{\mathbf{e}}_\rho(s,\theta) = -\kappa(s)\cos[\theta - \int_0^s \tau(s)ds]\hat{\mathbf{t}}(s)$ [13], where $\kappa(s)$ and $\tau(s)$ are the curvature and torsion of the centerline, respectively. This parametrization does not allow for jumps in $\rho(s)$ or blunt ends, similar to such as in many SBTs.

Assuming that the body does not change its volume, the flow around the body $\mathbf{u}(\mathbf{x})$ can be described through the single-layer boundary integral representation for incompressible Stokes flow. For an isolated body this representation is given by

$$8\pi\mu\mathbf{u}(\mathbf{x}) = \int_{-1}^{1} ds' \int_{-\pi}^{\pi} d\theta' \left(\frac{\mathbf{I}}{|\mathbf{R}'|} + \frac{\mathbf{R}'\mathbf{R}'}{|\mathbf{R}'|^3}\right) \cdot \mathfrak{f}(s',\theta'), \tag{2}$$

where $\mathbf{R}' = \mathbf{x} - \mathbf{S}(s', \theta')$ is a vector from the surface to the point of interest in the fluid, $\mathbf{I}$ is the identity matrix, μ is the viscosity of the fluid, and $\mathfrak{f}(s, \theta)$ is the fluid traction on the body multiplied by the integration surface element. This equation determines the flow both inside and outside the body. In the limit $\mathbf{x} \to \mathbf{S}(s, \theta)$, Eq. (2) becomes

$$8\pi\mu\mathbf{U}(s,\theta) = \int_{-1}^{1} ds' \int_{-\pi}^{\pi} d\theta' \left(\frac{\mathbf{I}}{|\mathbf{R}|} + \frac{\mathbf{R}\mathbf{R}}{|\mathbf{R}|^3} \right) \cdot \mathfrak{f}(s', \theta'), \tag{3}$$

where $\mathbf{U}(s, \theta)$ is the surface velocity of the body and $\mathbf{R} = \mathbf{S}(s, \theta) - \mathbf{S}(s', \theta')$. The above equation is a well-studied integral equation for $\mathfrak{f}(s', \theta')$ [24].

The integrand of the above equation blows up when $(s', \theta') = (s, \theta)$. This divergence can be removed by adding and subtracting another geometry with a known solution that cancels with the kernel at the said point. This process is reminiscent to that used by Batchelor in the development of his SBT [25]. We chose to add and subtract the flow around a translating spheroid with the symmetry axis aligned with the body tangent $\hat{\mathbf{t}}(s)$ at s. This spheroid has three unset geometric parameters: the distance from the center to the pole along the symmetry axis a, the equatorial radius ϵc, and the distance from the center to as_e [Fig. 1(b)]. These parameters should be chosen to match the tubular-body surface and tangent plane at $(s', \theta') = (s, \theta)$ to provide the best regularization of the integral kernel. This gives the effective spheroid the parametrization,

$$\mathbf{S}_e(s', \theta', s, \theta) = \mathbf{r}_e(s', s, \theta) + \epsilon\rho_e(s', s)\hat{\mathbf{e}}_\rho(s, \theta') + \mathbf{r}(s), \tag{4}$$

where $\mathbf{r}_e(s', s, \theta) = a(s, \theta)[s' - s_e(s)]\hat{\mathbf{t}}(s)$, $\rho_e(s', s) = c(s)\sqrt{1 - s'^2}$, $2c(s)^2 = \rho^2(s) + \rho(s)\sqrt{\rho^2(s) + 4[\partial_s\rho(s)]^2}$, $a(s, \theta) = 1 - \hat{\mathbf{t}}(s) \cdot \partial_s\hat{\mathbf{e}}_\rho(s, \theta)$, and $s_e(s) = \rho(s)\partial_s\rho(s)/c^2$. This geometry corresponds to a prolate spheroid if $\alpha = \epsilon c/a < 1$ and an oblate spheroid if $\alpha = \epsilon c/a > 1$. It satisfies $\mathbf{S}_e(s_e, \theta) = \mathbf{S}(s, \theta)$, $\partial_{s_e}\mathbf{S}_e(s_e, \theta) = \partial_s\mathbf{S}(s, \theta)$, and $\partial_\theta\mathbf{S}_e(s_e, \theta) = \partial_\theta\mathbf{S}(s, \theta)$, thereby replicating the position and tangent plane to the surface at (s, θ). Furthermore, it relaxes the typical SBT assumption on the curvature ($\epsilon\kappa \ll 1$) and assumes that the cross section satisfies $\rho(s)\partial_s\rho(s) \to$ constant as $\partial_s\rho(s) \to \infty$. The latter condition allows TBT to model rapidly changing cross sections provided $\partial_s\rho(s) \neq \infty$ away from ends and different types of ends that satisfy the criteria. The traction, multiplied by the surface element from the translational motion of a spheroid in a viscous fluid is constant for the above parametrization [26,27], and the total force from the motion is known. Hence, the boundary integral equation, Eq. (3), after adding and subtracting the effective geometry, can be written as

$$8\pi\mu\mathbf{U}(s,\theta) = \int_{-1}^{1} ds' \int_{-\pi}^{\pi} d\theta' [\mathbf{G} \cdot \mathfrak{f}(s', \theta') - \mathbf{G}_e \cdot \mathfrak{f}(s, \theta)] + \mathbf{M}'_A(s, \theta) \cdot \mathfrak{f}(s, \theta), \tag{5}$$

where $\mathbf{R}_e = \mathbf{S}_e[s_e(s), \theta, s, \theta] - \mathbf{S}_e(s', \theta', s, \theta)$, $\beta(s, \theta) = \alpha^2(s, \theta) - 1$,

$$\mathbf{G}_{(e)}(s', \theta', s, \theta) = \frac{\mathbf{I}}{|\tilde{\mathbf{R}}_{(e)}|} + \frac{\mathbf{R}_{(e)}\mathbf{R}_{(e)}}{|\tilde{\mathbf{R}}_{(e)}|^3}, \tag{6}$$

$$\mathbf{M}'_A(s, \theta) = \zeta'_\parallel(s, \theta)\hat{\mathbf{t}}(s)\hat{\mathbf{t}}(s) + \zeta'_\perp(s, \theta)[\mathbf{I} - \hat{\mathbf{t}}(s)\hat{\mathbf{t}}(s)], \tag{7}$$

$$\frac{a\beta^{3/2}}{4\pi}\zeta'_\parallel(s, \theta) = [(\beta - 1)\arccos(\alpha^{-1}) + \sqrt{\beta}], \tag{8}$$

$$\frac{a\beta^{3/2}}{2\pi}\zeta'_\perp(s, \theta) = [(3\beta + 1)\arccos(\alpha^{-1}) - \sqrt{\beta}], \tag{9}$$

and the subscript (e) means the notation applies for both the tubular body (no subscript) and the spheroid (subscript e) terms. In the above representation the singular point of the original kernel, located at $(s', \theta') = (s, \theta)$, cancels with the singular point of the spheroid kernel, located at $(s', \theta') = (s_e, \theta)$.

The cancellation of the singular point in Eq. (5) allows the integrands to be expanded. This expansion should move all the θ' dependences to the numerators of the integrands so that the angular dependence can be separated from the leading-order term [13]. This can be performed with the binomial series,

$$(1+x)^{\alpha} = \sum_{k=0}^{\infty} \binom{\alpha}{k} x^k, \tag{10}$$

where the generalized binomial coefficient is

$$\binom{\alpha}{k} = \frac{1}{k!} \prod_{n=0}^{k+1} (\alpha - n). \tag{11}$$

This series converges absolutely for $|x| < 1$ and $\alpha \in \mathbb{C}$ as the absolute value of each term is smaller than the previous one. The binomial series can be applied to the denominators of our integrands by defining $|\mathbf{R}_{(e)}|^2 = |\tilde{\mathbf{R}}_{(e)}|^2(1 + \delta\mathbf{R}_{(e)})$ where

$$|\tilde{\mathbf{R}}_{(e)}|^2 = \mathbf{R}_{0(e)}^2 + \epsilon^2 \rho_{(e)}(s_{(e)})^2 + \epsilon^2 \rho_{(e)}(s')^2, \tag{12}$$

$$\begin{aligned} |\tilde{\mathbf{R}}_{(e)}|^2 \delta\mathbf{R}_{(e)} = &-2\epsilon^2 \rho_{(e)}(s_{(e)})\rho_{(e)}(s')\hat{\mathbf{e}}_{\rho}(s_{(e)}, \theta) \cdot \hat{\mathbf{e}}_{\rho}(s', \theta') + 2\epsilon \rho_{(e)}(s_{(e)})\mathbf{R}_{0(e)} \cdot \hat{\mathbf{e}}_{\rho}(s_{(e)}, \theta) \\ &- 2\epsilon \rho_{(e)}(s')\mathbf{R}_{0(e)} \cdot \hat{\mathbf{e}}_{\rho}(s', \theta'). \end{aligned} \tag{13}$$

Equation (12) is the sum of the squared lengths of each vector within $\mathbf{R}_{(e)}$ and does not depend on θ' whereas Eq. (13) is the cross-vector terms occurring within $|\mathbf{R}_{(e)}|^2$ and so has dependence on (s, s', θ, θ'). The triangle inequality tells us that $|\mathbf{R}_{(e)}|^2 \leqslant |\tilde{\mathbf{R}}_{(e)}|^2$ and so $|\delta\mathbf{R}_{(e)}| \leqslant 1$. Furthermore, $|\delta\mathbf{R}_{(e)}| = 1$ iff $(s', \theta') = (s, \theta)$, but this point was removed by the above regularization. Hence, we can produce a binomial series in $\delta\mathbf{R}_{(e)}$ to express the boundary integral as

$$\begin{aligned} 8\pi\mu\mathbf{U}(s,\theta) = &\sum_{k=0}^{\infty} \int_{-1}^{1} ds' \int_{-\pi}^{\pi} d\theta' \delta\mathbf{R}^k \mathbf{G}^{(k)} \cdot \mathfrak{f}(s', \theta') - \sum_{k=0}^{\infty} \int_{-1}^{1} ds' \int_{-\pi}^{\pi} d\theta' \delta\mathbf{R}_e^k \mathbf{G}_e^{(k)} \cdot \mathfrak{f}(s, \theta) \\ &+ \mathbf{M}_A'(s, \theta) \cdot \mathfrak{f}(s, \theta), \end{aligned} \tag{14}$$

where $\mathbf{R}_{0(e)} = \mathbf{r}_{(e)}(s_{(e)}) - \mathbf{r}(s')$, and

$$\mathbf{G}_{(e)}^{(k)}(s', \theta', s, \theta) = \binom{-\frac{1}{2}}{k} \frac{\mathbf{I}}{|\tilde{\mathbf{R}}_{(e)}|} + \binom{-\frac{3}{2}}{k} \frac{\mathbf{R}_{(e)}\mathbf{R}_{(e)}}{|\tilde{\mathbf{R}}_{(e)}|^3}. \tag{15}$$

This binomial series converges absolutely provided $\delta\mathbf{R}_{(e)} < 1$. This is true everywhere except at the singular point $(s', \theta') = (s, \theta)$. At this point, however, the individual terms from the body and spheroid cancel. Hence, this expanded representation is exact.

The $k = 0$ terms in the above series are larger than any other term in the summation. This is because when $|\delta\mathbf{R}_{(e)}| < 1$, each subsequent term in the series is smaller than the last and when $|\delta\mathbf{R}_{(e)}| = 1$, each k of the body cancels with its spheroid counterpart. Hence, we could assume that the $k \neq 0$ and the angular-dependent terms within $k = 0$ are "relatively small" and group them together. This turns the equation into

$$8\pi\mu\mathbf{U}(s,\theta) = \int_{-1}^{1} ds' \int_{-\pi}^{\pi} d\theta' [\mathbf{K} \cdot \mathfrak{f}(s', \theta') - \mathbf{K}_e \cdot \mathfrak{f}(s, \theta)] + \varepsilon \Delta\mathcal{L}[\mathfrak{f}](s, \theta) + \mathbf{M}_A'(s, \theta) \cdot \mathfrak{f}(s, \theta), \tag{16}$$

where

$$\mathbf{K}_{(e)} = \frac{\mathbf{I}}{|\tilde{\mathbf{R}}_{(e)}|} + \frac{\mathbf{R}_{0(e)}\mathbf{R}_{0(e)}}{|\tilde{\mathbf{R}}_{(e)}|^3}, \tag{17}$$

$$\varepsilon\, \Delta\mathcal{L}[\mathfrak{f}](s, \theta) = \int_{-1}^{1} ds' \int_{-\pi}^{\pi} d\theta' (\mathbf{G} - \mathbf{K}) \cdot \mathfrak{f}(s', \theta') - \int_{-1}^{1} ds' \int_{-\pi}^{\pi} d\theta' (\mathbf{G}_e - \mathbf{K}_e) \cdot \mathfrak{f}(s, \theta), \tag{18}$$

and ε is the small parameter representing the size of the angular and $k \neq 0$ terms. In the above, $\varepsilon\,\Delta\mathcal{L}[\mathfrak{f}]$ is a surface integral operator that contains all the $k \neq 0$ and angular terms that are assumed small. It is equivalent to the boundary integral of the tubular body without the corresponding $k = 0$ term minus the boundary integral of the spheroid without the $k = 0$ term because of the convergence of the binomial series. The latter interpretation is the easier way to evaluate this term when $\mathfrak{f}$ is known. It is not clear, *a priori*, that $\varepsilon\,\Delta\mathcal{L}[\mathfrak{f}]$ is small, but we note that its integrand cancels as $(s', \theta') \to (s, \theta)$ and is small when (s', θ') far from (s, θ) ($\delta R \ll 1$). This representation suggests expanding $\mathfrak{f}(s, \theta)$ as

$$\mathfrak{f}(s, \theta) = \sum_{n=0}^{\infty} (-1)^n \varepsilon^n \mathfrak{f}_n(s, \theta), \tag{19}$$

and collecting like powers of ε. Hence, $\mathfrak{f}_n(s, \theta)$ satisfies

$$8\pi\mu \mathbf{U}(s, \theta) = \int_{-1}^{1} ds' \mathbf{K}(s', s) \cdot \langle \mathfrak{f}_0(s', \theta') \rangle_{\theta'} + \mathbf{M}_A(s, \theta) \cdot \mathfrak{f}_0(s, \theta), \tag{20}$$

$$\Delta\mathcal{L}[\mathfrak{f}_{n-1}](s, \theta) = \int_{-1}^{1} ds' \mathbf{K}(s', s) \cdot \langle \mathfrak{f}_n(s', \theta') \rangle_{\theta'} + \mathbf{M}_A(s, \theta) \cdot \mathfrak{f}_n(s, \theta). \tag{21}$$

Equations (19)–(21) form the tubular-body theory equations. In them we have evaluated the $k = 0$ spheroid integrals [28] and defined $\langle(\cdot)\rangle_{\theta'} = \int_{-\pi}^{\pi}(\cdot)d\theta'$,

$$\mathbf{M}_A(s, \theta) = \{\zeta_{\parallel}(s, \theta)\hat{\mathbf{t}}(s)\hat{\mathbf{t}}(s) + \zeta_{\perp}(s, \theta)[\mathbf{I} - \hat{\mathbf{t}}(s)\hat{\mathbf{t}}(s)]\}, \tag{22}$$

$$\zeta_{\parallel}(s, \theta) = \zeta_{\parallel}' - \frac{1 - \beta}{a(-\beta)^{3/2}} L - g(1, s, \theta) + g(-1, s, \theta), \tag{23}$$

$$\zeta_{\perp}(s, \theta) = \zeta_{\perp}' - \frac{1}{a\sqrt{-\beta}} L, \tag{24}$$

$$L(s, \theta) = \ln\left(\frac{a(s_e - \beta) + \sqrt{-\beta}|\tilde{\mathbf{R}}_e|(-1)}{a(s_e + \beta) + \sqrt{-\beta}|\tilde{\mathbf{R}}_e|(1)}\right), \tag{25}$$

$$g(s', s, \theta) = \frac{2(s_e - s')}{\beta|\tilde{\mathbf{R}}_e|(s', s, \theta)}\left(\frac{s' s_e \alpha^2 - (1 - s_e^2)\beta}{2\beta - s_e^2(1 - \beta)}\right). \tag{26}$$

Importantly, this series representation is exact and converges provided $|\mathfrak{f}_{n-1}| > |\mathfrak{f}_n|$. The proof of this is beyond the scope of this paper, but we note that this condition was satisfied in all our tests as $\varepsilon\,\Delta\mathcal{L}[\mathfrak{f}](s, \theta)$ was found to be small.

The TBT integral operator, present in Eqs. (20) and (21), is similar to a SBT operator but involves both s and θ. However, averaging over this θ component it can be rewritten as

$$\left\langle \mathbf{M}_A^{-1} \cdot \mathbf{q}(s, \theta) \right\rangle_{\theta} = \left\langle \mathbf{M}_A^{-1} \right\rangle_{\theta} \cdot \int_{-1}^{1} ds' \mathbf{K} \cdot \langle \mathfrak{f}(s', \theta') \rangle_{\theta'} + \langle \mathfrak{f}(s, \theta') \rangle_{\theta'}, \tag{27}$$

$$\mathfrak{f}(s, \theta) = \mathbf{M}_A^{-1} \cdot \mathbf{q}(s, \theta) - \mathbf{M}_A^{-1} \cdot \left\langle \mathbf{M}_A^{-1} \right\rangle_{\theta}^{-1} \cdot \left\langle \mathbf{M}_A^{-1} \cdot \mathbf{q}(s, \theta) \right\rangle_{\theta} + \mathbf{M}_A^{-1} \cdot \left\langle \mathbf{M}_A^{-1} \right\rangle_{\theta}^{-1} \cdot \langle \mathfrak{f}(s, \theta') \rangle_{\theta'} \tag{28}$$

where $\mathbf{q}(s, \theta)$ represents the known functions on the left-hand sides of Eqs. (20) and (21) . The above expression shows that solutions to the TBT operator are equivalent to a Fredholm integral equation of the second kind and a sequence of matrix operations. Furthermore, the kernel of this integral operator is compact and self-adjoint. These kinds of Fredholm equations are well posed and diagonalizable [29]. As such, there are several ways to solve these problems numerically, and analytical solutions can be expressed as in an infinite series of integrals (see the Supplemental Material (SM) [29,30]). The structure of these kernels is also close to the modified SBT of Tornberg

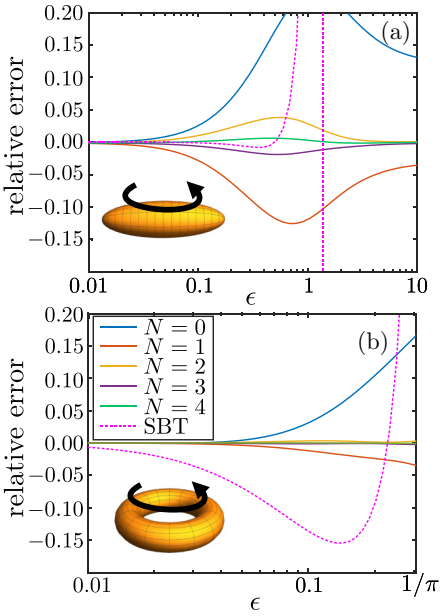

FIG. 2. The relative error between TBT and the exact solution for torque from the (a) broadwise rotation of a prolate spheroid and the (b) axisymmetric rotation or torus. The relative error is defined as the difference between the prediction and the exact coefficient divided by the exact coefficient. Different lines correspond to the TBT prediction with different levels of truncation; blue is the leading term ($N = 0$), red is the first two terms ($N = 1$), yellow is the first three ($N = 2$), purple is the first four ($N = 3$), and green is the first five ($N = 4$). The pink dashed line is the SBT approximation.

and Shelley [10] and the SBT of Andersson *et al.* [15] both of which have positive definite eigenvalues.

III. VALIDATION

We solved the TBT integral equations, Eqs. (20) and (21) with a collocation method [29] and truncated the series in Eq. (19) at $n = N$. Briefly the collocation method divides $s \in [-1, 1]$ into segments and assumes $\mathfrak{f}$ is constant over each segment. Equation (27) is then turned into a system of linear equations by enforcing that they hold at the center of each segment (full details provided in the SM [31] and Refs. [8,29,32]). We note that this simple collocation implementation is possible because the integral kernel in Eq. (27) is compact unlike in Keller and Rubinow's SBT [11].

The accuracy of the TBT equations, Eqs (19)–(21), was tested against the solutions for the drag on a spheroid [33] and a torus [34–36] for a wide range of ϵs. The terms with the largest relative error are shown in Fig. 2 (other terms available in the SM [37] and Refs. [33–36,38–41]). The translation coefficients for the spheroid were found to capture the behavior exactly over the entire range considered. This is because we used the solution for a translating spheroid as the effective geometry. The relative error between the known solutions and that predicted by the TBT decreases as the number of terms kept in Eq. (19) increases (Fig. 2). At leading order ($N = 0$) the largest error is around 20% and occurs when the spheroid is almost spherical, $\epsilon \sim 1$ and the torus is closed $\epsilon = 1/\pi$. Both of these cases lie well outside the typical SBT limits. When $\epsilon \sim 1$ the body is not slender whereas when $\epsilon = 1/\pi$ the curvature of the torus equals the thickness. This relative error decreases to less than 1% after including the first five terms ($N = 4$) in Eq. (19) for the entire region tested. The convergence of the TBT, over a range much larger then available to classical

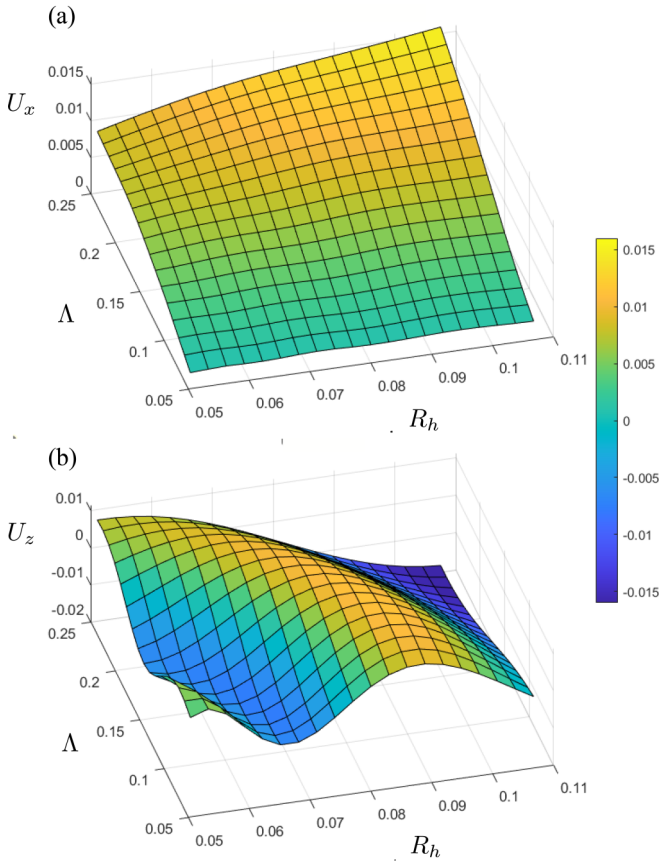

FIG. 3. The translational velocity of a force-free helix from rotation around its axis (x axis). (a) velocity along its axis (U_x), (b) velocity perpendicular to axis (U_z). All plots are shown for $\epsilon = 0.05$.

SBT, suggests that the TBT could prove effective when determining the viscous hydrodynamics of cablelike bodies in complex situations.

The power of the TBT can be further demonstrated using a tightly wound helix [Fig. 1(a)]. Helices are iconic in slow-viscous flow and occur in many mechanical and biological situations. Although common, relatively little is known about how the dynamics of these helices change as they become tightly wound, even though some micro-organisms form these tightly wound helical shapes [42]. One possible explanation of this is because such shapes lie well outside the SBT limits and so full numerical simulations would be needed. The TBT, however, is exact and so can be used in these limits.

We investigated the velocity of a force-free helix which is rotated around its central axis (Fig. 3), varying the helix pitch, Λ, and radius R_h (Fig. 1). The parametrization used and resistance matrix of the said helix is available in the SM [43]. In this example we restricted ourselves to inextensible helices with $\epsilon = 0.05$. The geometric constraint that the helix does not touch itself means $\Lambda, R_h > \epsilon$. For these bodies, Eq. (19) had converged by $N = 6$. Over the range tested, the velocity of the helix along its axis increases as Λ and R_h increases [Fig. 3(a)]. This is probably due to the coupling between translation and rotation increasing as the helix becomes less coiled. The velocity perpendicular to the helix axis, however, displays nontrivial oscillatory behavior [Fig. 3(b)]. Hence, although these bodies are very tightly wound, the system still experiences nontrivial effects from its helical shape.

IV. DISCUSSION AND CONCLUSION

Fiberlike objects occur in many interesting and important situations but can be tricky to model theoretically. Direct numerical simulations typically require high levels of resolution, whereas the asymptotic slender-body theories are restricted to leading-order solutions in specific regimes. The extension of these SBTs beyond these approximation limits has, therefore, been identified as a key problem for several interdisciplinary research fields [1–5,9,10,20,22,23].

This paper develops tubular-body theory; a SBT-like theory that can determine the traction on cablelike bodies exactly. TBT expresses the surface traction on the body as the sum of solutions to a one-dimensional integral equation [Eqs. (19)–(21)]. This integral equation is similar to that developed in the SBT except with a compact and self-adjoint integral operator. These types of integral equations are called Fredholm integral equations of the second kind and have been studied extensively. Furthermore Fredholm integral equations of the second with compact and self-adjoint operators are well posed and diagonalizable. As such there exists several methods to solve them both numerically and theoretically [29].

We used a collocation method to numerically solve these equations. The compact nature of the integral operator means this representation does not suffer from issues with the kernel blowing up. We then compared the predictions of the TBT to the exact solutions for drag on a spheroid and a torus. In both cases we found that with only the first five terms in the series, the TBT was able to determine the resistance coefficients to within 1% error. This was tested for spheroids ranging from the very slender/prolate ($\epsilon = 0.01$) to very oblate ($\epsilon = 10$) and tori ranging from slender ($\epsilon = 0.01$) to closed ($\epsilon = 1/\pi$). We then used the TBT to look at the velocity of a rotating force-free tightly wound helix, observing that even in these tightly wound shapes the helix showed nontrivial dependence on the geometry.

In addition to being exact, the TBT has several useful properties, and its derivation can be generalized to more complicated geometries. The ability of the TBT to resolve the traction on the body means the force and torque on the body in any flow can be determined from the Lorentz reciprocal relationship and the results for rigid body motion [8]. This process is useful for determining the swimming of microscopic organisms and asymptotically interacting bodies through the method of reflections [8,26]. Furthermore, the equations can be extended to filamentous bodies near (but not touching) walls or other objects by including the appropriate corrections to the single-layer boundary integral representation [24]. This is because these terms do not introduce any new singular points in the Green's function when evaluated on the surface of the body and so the binomial series treatment holds. An improved effective geometry Eq. (4) may, however, improve the convergence of the final series representation.

Finally we note that, although we have focused on fibers in viscous flow, the derivation can be easily repeated for several other systems. The derivation itself relies on three elements: a boundary integral representation for the system, the known solution for spheroidal geometries, and the binomial series. Thankfully many systems of interest, such as diffusion, satisfy these conditions with the behavior of ellipsoids often being a solved geometry.

ACKNOWLEDGMENTS

L.K. was funded by the Australian Research Council (ARC) under the Discovery Early Career Research Award Scheme (Grant Agreement No. DE200100168).

[1] E. Lauga, Bacterial Hydrodynamics, Annu. Rev. Fluid Mech. **48**, 105 (2016).

[2] E. A. Gaffney, H. Gadêlha, D. J. Smith, J. R. Blake, and J. C. Kirkman-Brown, Mammalian sperm motility: Observation and theory, Annu. Rev. Fluid Mech. **43**, 501 (2011).

[3] E. Nazockdast, A. Rahimian, D. Zorin, and M. Shelley, A fast platform for simulating semi-flexible fiber suspensions applied to cell mechanics, J. Comput. Phys. **329**, 173 (2017).
[4] B. Ruzicka and E. Zaccarelli, A fresh look at the Laponite phase diagram, Soft Matter **7**, 1268 (2011).
[5] M. R. Sanjay, P. Madhu, M. Jawaid, P. Senthamaraikannan, S. Senthil, and S. Pradeep, Characterization and properties of natural fiber polymer composites: A comprehensive review, J. Cleaner Prod. **172**, 566 (2018).
[6] L. M. Lemma, M. M. Norton, A. M. Tayar, S. J. DeCamp, S. A. Aghvami, S. Fraden, M. F. Hagan, and Z. Dogic, Multiscale Microtubule Dynamics in Active Nematics, Phys. Rev. Lett. **127**, 148001 (2021).
[7] L. Koens and T. D. Montenegro-Johnson, Local drag of a slender rod parallel to a plane wall in a viscous fluid, Phys. Rev. Fluids **6**, 064101 (2021).
[8] S. Kim and S. J. Karrila, *Microhydrodynamics: Principles and Selected Applications* (Courier, Boston, 2005).
[9] O. du Roure, A. Lindner, E. N. Nazockdast, and M. J. Shelley, Dynamics of flexible fibers in viscous flows and fluids, Annu. Rev. Fluid Mech. **51**, 539 (2019).
[10] A. Tornberg and M. J. Shelley, Simulating the dynamics and interactions of flexible fibers in Stokes flows, J. Comput. Phys. **196**, 8 (2004).
[11] J. B. Keller and S. I. Rubinow, Slender-body theory for slow viscous flow, J. Fluid Mech. **75**, 705 (1976).
[12] R. E. Johnson, An improved slender-body theory for Stokes flow, J. Fluid Mech. **99**, 411 (1979).
[13] L. Koens and E. Lauga, The boundary integral formulation of Stokes flows includes slender-body theory, J. Fluid Mech. **850**, R1 (2018).
[14] T. Götz, Interactions of fibers and flow: Asymptotics, theory and numerics, Ph.D. thesis, University of Kaiserslautern, Kaiserslautern, Germany, 2000.
[15] H. I. Andersson, E. Celledoni, L. Ohm, B. Owren, and B. K. Tapley, An integral model based on slender body theory, with applications to curved rigid fibers, Phys. Fluids **33**, 041904 (2021).
[16] E. Barta and N. Liron, Slender body interactions for low reynolds numbers-part I: Body-wall interactions, SIAM J. Appl. Math. **48**, 992 (1988).
[17] S. Gueron and N. Liron, Ciliary motion modeling, and dynamic multicilia interactions, Biophys. J. **63**, 1045 (1992).
[18] J. J. L. Higdon, A hydrodynamic analysis of flagellar propulsion, J. Fluid Mech. **90**, 685 (1979).
[19] Y. Man, L. Koens, and E. Lauga, Hydrodynamic interactions between nearby slender filaments, Europhys. Lett. **116**, 24002 (2016).
[20] C. Brennen and H. Winet, Fluid mechanics of propulsion by cilia and flagella, Annu. Rev. Fluid Mech. **9**, 339 (1977).
[21] P. Katsamba, S. Michelin, and T. D. Montenegro-Johnson, Slender phoretic theory of chemically active filaments, J. Fluid Mech. **898**, A24 (2020).
[22] S. K. Kugler, A. Kech, C. Cruz, and T. Osswald, Fiber orientation predictions-a review of existing models, J. Compos. Sci. **4**, 69 (2020).
[23] P. M. Reis, F. Brau, and P. Damman, The mechanics of slender structures, Nat. Phys. **14**, 1150 (2018).
[24] C. Pozrikidis, *Boundary Integral and Singularity Methods for Linearized Viscous Flow* (Cambridge University Press, Cambridge, UK, 1992).
[25] G. K. Batchelor, Slender-body theory for particles of arbitrary cross-section in Stokes flow, J. Fluid Mech. **44**, 419 (1970).
[26] H. Brenner, The Stokes resistance of an arbitrary particle, Chem. Eng. Sci. **18**, 1 (1963).
[27] C. P. Martin, Surface tractions on an ellipsoid in Stokes flow: Quadratic ambient fields, Phys. Fluids **31**, 021209 (2019).
[28] I. S. Gradshteyn, I. M. Ryzhik, A. Jeffrey, and D. Zwillinger, *Table of Integrals, Series, and Products* (Academic, San Diego, 2000).
[29] A. D. Polianin and A. V. Manzhirov, *Handbook of Integral Equations*, 2nd ed. (Chapman & Hall/CRC, Boca Raton, FL, 2008).
[30] See Supplemental Material at http://link.aps.org/supplemental/10.1103/PhysRevFluids.7.034101 for the explicit analytical solution to the tubular-body equations.

[31] See Supplemental Material at http://link.aps.org/supplemental/10.1103/PhysRevFluids.7.034101 for a detailed description of the numerical method.
[32] MATLAB, version 9.10.0.1710957 (R2021a) (The MathWorks, Natick, MA, 2021).
[33] H. Lamb, *Hydrodynamics*, 6th ed. (Cambridge University Press, Cambridge, UK, 1932).
[34] W. H. Pell and L. E. Payne, On Stokes flow about a torus, Mathematika **7**, 78 (1960).
[35] R. P. Kanwal, Slow steady rotation of axially symmetric bodies in a viscous fluid, J. Fluid Mech. **10**, 17 (1961).
[36] S. R. Majumdar and M. E. O'Neill, On axisymmetric stokes flow past a torus, Zeitschrift für Angew. Math. und Phys. ZAMP **28**, 541 (1977).
[37] See Supplemental Material at http://link.aps.org/supplemental/10.1103/PhysRevFluids.7.034101 for the other resistance coefficients for the sphereoid and the torus.
[38] L. Koens and E. Lauga, The passive diffusion of Leptospira interrogans, Phys. Biol. **11**, 066008 (2014).
[39] R. E. Johnson and T. Y. Wu, Hydromechanics of low-Reynolds-number flow. Part 5. Motion of a slender torus, J. Fluid Mech. **95**, 263 (1979).
[40] J. M. Dorrepaal, S. R. Majumdar, M. E. O'Nejll, and K. B. Ranger, A closed torus in stokes flow, Q. J. Mech. Appl. Math. **29**, 381 (1976).
[41] S. R. Majumdar and M. E. O'Neill, Asymmetric stokes flows generated by the motion of a closed torus, Zeitschrift für Angew. Math. und Phys. ZAMP **30**, 967 (1979).
[42] K. Young, The selective value of bacterial shape., Microbiol. Mol. Biol. Rev. **70**, 660 (2006).
[43] See Supplemental Material at http://link.aps.org/supplemental/10.1103/PhysRevFluids.7.034101 for parametrization used and resistance matrix of said helix is available.